Linear $\ell = 1$ Stellarator Experiments Using a Shaped Coil

E. Fünfer, M. Kaufmann, W. Lotz,
J. Neuhauser, G. Schramm and U. Seidel

IPP 1/130 February 1973

MAX-PLANCK-INSTITUT FÜR PLASMAPHYSIK

GARCHING BEI MÜNCHEN

MAX-PLANCK-INSTITUT FÜR PLASMAPHYSIK

GARCHING BEI MÜNCHEN

Linear $\ell = 1$ Stellarator Experiments Using a Shaped Coil

E. Fünfer, M. Kaufmann, W. Lotz,
J. Neuhauser, G. Schramm and U. Seidel

IPP 1/130 February 1973

Die nachstehende Arbeit wurde im Rahmen des Vertrages zwischen dem Max-Planck-Institut für Plasmaphysik und der Europäischen Atomgemeinschaft über die Zusammenarbeit auf dem Gebiete der Plasmaphysik durchgeführt.

IPP 1/130

E. Fünfer
M. Kaufmann
W. Lotz
J. Neuhauser
G. Schramm
U. Seidel

Linear $\ell = 1$ Stellarator Experiments Using a Shaped Coil.

(in English)

February 1973

Abstract

Linear theta pinch experiments on ISAR I with superposed helical $\ell = 1$ field are reviewed. The helical magnetic field is generated by shaping the main theta coil, in contrast to a preceding experiment on the same bank [1]. Equilibrium and stability of the helical pinch are studied over a wide range of plasma parameters.

The helical equilibrium is found to be in reasonable agreement with existing theories.

Short wavelength helical m = 1 oscillations are observed in connection with the helix formation. The strong damping of these oscillations (Alfvén waves) is explained in terms of phase mixing as a consequence of the diffuse density profile.

Long wavelength m = 1 instabilities are observed for $\beta \gtrsim 0.4$. Their growth rates are in reasonable agreement with sharp boundary theory if the ends are assumed to be fixed.

$m \geq 2$ perturbations produced by the fast compression are damped away in the adiabatic phase, i. e. these modes are not unstable modes of the static equilibrium.

Contents:

A. Introduction

In a preceding report /1/ we described linear θ-pinch experiments with superposed helical fields generated with helical wires. These experiments were continued on the same ISAR I 2.6 MJ bank using a shaped coil, that is, the helical field was generated by appropriately shaping the inner surface of the 5.4 m long theta pinch coil. The results of the latter investigations are given in the following paper. Some details may also be found in /2, 3/.

All the experiments in straight helical geometry are concentrated on $\ell = 1$ helical symmetry because the $\ell = 1$ system should be nearly stable with respect to the most dangerous $m = 1$ mode or at least exhibits the lowest growth rate. At high beta wall stabilization should be possible /4/. The linear experiments are preparatory to a big toroidal experiment (2.7 m diameter), again on the ISAR I bank, where helical fields will be used to compensate the toroidal drift force /5, 25/.

The vacuum magnetic field produced by the helical system is of the same type as in the well-known low-beta stellarator and, consequently, we refer to the helical theta pinch as a high-beta stellarator.
Nevertheless, we emphasize that such high-beta equilibria are quite different from low-beta stellarator equilibria, the basic mechanism for toroidal equilibrium being M & S -like [26] rather than of the stellarator type.
In detail, we have investigated the following three modifications with shaped coil:
In the first experiment, we used the same small cylindrical discharge tube as in the earlier experiment with helical wires. We were thus able to compare the plasma behaviour for the two different methods of field generation for nearly identical plasma parameters.

Next the same small discharge tube was placed in an eccentric position relative to the coil axis, which is identical with the axis of symmetry of the helical system. Such an asymmetric position may simulate the situation in toroidal geometry if the plasma is drifting or is generated away from the equilibrium position. This may also afford a first idea of the stability of the helical theta pinch, even with low temperature, because of the large initial deviation from equilibrium.

In the last version a large diameter cylindrical discharge tube which just fitted into the shaped coil was used. In this case the initial shock heating was much more effective and therefore a higher temperature (a few keV) was achieved.

The gross magnetic field in the shaped coil was only slightly different from that in the original theta coil. In previous pure theta pinch experiments the same two discharge tubes were used. In so far as plasma parameters were not remeasured with the shaped coil, they were estimated from these older theta pinch results.

Similar experiments with helical geometry have been conducted at Los Alamos /6/.

B. Vacuum magnetic field

The pulsed helical field can be generated in different ways. In our first version, called experiment I in the following, we used helical wires inside the usual cylindrical theta coil. The helical field could thus be varied independently of the main longitudinal field. Simple field programming was also possible by independently firing the two banks.

In the experiments described below the inner surface of the theta coil was shaped approximately as a flux surface of a $\ell = 1$ stellarator. For technical reasons the helical surface was approximated with narrow circular cylinders the center of which lay on a helix with a period length of 60 cm and a radius of 1.5 cm (20 steps per period; see Fig. 1).

Apart from technical difficulties and variability, the difference between the two systems is given by the different amount of helical harmonics generated by the special current distribution or the shaped coil surface, resulting in, for instance, the existence or non-existence of a separatrix (see below). The vacuum magnetic field in helical geometry can be described by a scalar potential using cylindrical coordinates (r, θ, z):

$$\phi = a_0 z + \sum_{\ell=1}^{\infty} a_\ell \cdot \sin \ell(\theta - hz) \cdot I_\ell(\ell h r) \qquad (1)$$

$$\text{and} \qquad B = -\mu_0 \cdot \nabla \phi$$

$h = \frac{2\pi}{\lambda}$, λ = period length,

$a_o = \frac{B_{zo}}{\mu_o}$, I_ℓ, K_ℓ modified Bessel functions (standard notation).

1. Wires

For a single pair of helical conductors with equal but anti-parallel currents the coefficients a_ℓ are given by

$$a_\ell = 0 , \quad \ell = 2, 4, 6, \ldots$$

$$a_\ell \propto K_\ell'(r^*), \quad \ell = 1, 3, 5, \ldots ; \quad r^* = \ell h r_{wire}$$

(The prime always denotes differentiation with respect to the argument.) Therefore, the first and most important harmonic has $\ell = 3$. Because of the strong radial dependence this harmonic can, in general, be neglected for small r, but may be of the same order as the $\ell = 1$ contribution near the tube wall.

In addition, there is a weakening of the helical field by helical mirror currents induced in the main theta coil. For a single ℓ number this weakening inside the helical wires ($r < r_{wire}$) can

be described by a constant factor $S_\ell \leq 1$ of the form

$$S_\ell = 1 - \frac{I'_\ell(\ell hr_{wire}) \cdot K'_\ell(\ell hr_{wall})}{I'_\ell(\ell hr_{wall}) \cdot K'_\ell(\ell hr_{wire})}$$

For $\ell hr_{wall} \ll 1$ this reduces to the formula for the simple multipole configuration

$$S_\ell = 1 - \left(\frac{r_{wire}}{r_{wall}} \right)^{2\cdot\ell}$$

The weakening is stronger for lower ℓ numbers and, therefore, the relative content of harmonics is influenced by the wall distance. The content of harmonics can also be varied by using several wires in parallel instead of each single wire as was done in our first experiment /1/.

The radius of the separatrix always present in a wire stellarator is strongly affected by the harmonics and may be optimized by appropriately choosing the singularities.

2. Shaped coil

In the case of a shaped coil one has the boundary condition that for times short compared to the skin time of the coil the inner surface must be a flux surface. Again, one has to calculate the coefficients a_ℓ of (1). This problem is treated in /7/, which includes numerical results. If the local cross section of the shaped coil is circular, the most important harmonic is $\ell = 2$. Using the technical data given above, we find that, for instance, the radial magnetic field produced by the $\ell = 2$ component is at least one order of magnitude lower than the corresponding $\ell = 1$ contribution all over the cross section. Again, for $r = 0$ the harmonic field vanishes, whereas the $\ell = 1$ contribution remains finite.

In contrast to the wire stellarator, there is no separatrix in the vacuum field inside the shaped coil. This means that the

harmonics are set up in such a way that the separatrix vanishes for $r \leq r_{wall}$. We should mention that for a pure $\ell = 1$ (no harmonics) the separatrix is well defined and is determined by the helical wavelength and amplitude. Therefore, producing a pure $\ell = 1$ with a shaped coil would mean that the coil must have exactly the shape of a closed flux surface of the $\ell = 1$ located inside the separatrix, that is, the maximum average coil radius would be limited to the radius of the separatrix of the pure $\ell = 1$.

Calculating now the magnetic surfaces inside our shaped coil, we find that the flux tubes are not concentric /7/. The helical displacement away from the axis of symmetry increases with increasing diameter of the flux tube. In our case we chose a helical displacement of 1.5 cm for the inner surface of the coil, resulting in a helical amplitude of the magnetic axis of only $r_m = 0.94$ cm.

The rotational transform per period near the magnetic axis is constant for an $\ell = 1$ stellarator:

$$t_p = \frac{\iota_p}{2\pi} = \frac{1}{2} h^2 r_m^2$$

With $r_m = 0.94$ cm, $\lambda = 60$ cm, we get for the total length:

$$t_{total} \approx 0.045 ,$$

corresponding to a rotation of 16° between the ends of the coil.

If a high-beta plasma is now established near the axis of the helical field, then additional terms $\left(\propto K_\ell(\ell hr) \right)$ arise in the scalar potential because of helical mirror currents on the equilibrium plasma surface. New terms with strong radial dependence therefore appear in the expression for t, resulting in high shear near the plasma surface or in a diffuse plasma profile.

C. Related theta pinch experiments

Prior to the linear stellarator work on ISAR I we conducted linear theta pinch experiments using a coil with an inner diameter of 19.6 cm and a length of 5.4 m. This coil was also used later on for the linear experiment with helical wires and, finally, its inner surface was machined and shaped as a helical flux surface. In theta pinch as well as in stellarator experiments we worked with two different quartz tubes, the inner diameters being 8.5 cm and 17 cm respectively.
The gross plasma parameters in pure and modified theta pinches are mainly determined by the rise time and magnitude of the confining longitudinal field, by the diameter of the discharge tube, and by the filling pressure /8/.
Therefore, by choosing very similar sets of data in all the linear experiments we were able to compare the plasma behaviour, especially plasma stability, with and without helical fields under nearly identical conditions.

Results of the linear θ-pinch experiments can be found in /9-13/. In so far as plasma parameters were not remeasured in helical geometry, we used the corresponding θ-pinch values, keeping in mind the slightly increased inductance of the shaped coil.

D. Linear high-beta stellarator experiments with shaped coil

1. Survey

A comparison of the technical data and main plasma parameters of all linear stellarator experiments performed on ISAR I (August 1969 - September 1970) is given in Table 1. Standard plasma diagnostic methods were used in all experiments to derive the plasma parameters and to test plasma stability: The plasma motion was determined with smear pictures from a rotating mirror camera and image converter tubes. The density profile was measured with a calibrated camera and by means of the continuum radiation (10-channel apparatus) in a line-free interval.

The ion temperature was deduced from the neutron rate. The electron temperature was calculated from the intensity maxima of impurity lines (O,C), the corresponding rate equations being solved by iteration.
Compensated magnetic loops were used to measure the excluded flux.
The parameters of the thin plasma halo outside the dense column were examined by spectroscopic methods /14/. In the last experiment internal magnetic probe measurements were also performed.

In this report we are mainly concerned with the equilibrium and stability of the helical system. Therefore, plasma parameters are only given where necessary for comparison with the relevant theories.

The main result of exp. I was that shock heating also works in the presence of helical fields and that the helical equilibria predicted by theory can be achieved. The general plasma behaviour was very similar to that of the simple θ-pinch. Details can be found in /1/.

Exp. II, III, and IV are described in the following. The main results will be discussed in section E.

Table 1

Experiment No.	I	II	III	IV
Length of the coil	5.4 m			
Generation of $\ell = 1$ field	wires	shaped coil		
No. of periods	8	9		
Amplitude of magnetic axis	0 ...2 cm	0.94 cm		
Maximum magnetic field $B_{z,max}$	45 kG	40 kG		
Tube diameter	8.5 cm			17 cm
Tube position	concentric		eccentric	concentric
Density* on axis	a few 10^{16}			
Ion temperature*	...0.23 keV	... 0.6	... 0.4	0.05 ...2keV

* depending on filling pressure and bank energy used in the experiment in question.

2. Experiment II

In this experiment the same small discharge tube as in exp. I was used, but the helical field was generated by the shaped coil. The tube position was concentric with the helical system as in exp. I. Because of the higher inductance of the shaped coil the maximum magnetic field was about 10 % lower and the rise time somewhat longer. Therefore, starting with the same initial parameters in both cases, the temperature in exp. II was slightly lower than in exp. I, resulting in a small difference in the time scales. With this fact in mind, a direct comparison between exp. II and exp. I (simultaneously triggered main and helical fields) was possible.

The results of exp. II were as follows:

In the first discharges the z-pinch preionization had the same high energy and relatively long current pulse as in all the preceding linear experiments. In this case we observed a split-up of the plasma ($m \geq 2$), especially during the dynamic phase except at low filling pressure and high bank energy.

Later on the total width of the second current pulse of the preionization was reduced to only 2 µs (Fig. 1) and as a consequence the instability in the early phase was suppressed. With the reduced preionization plasma split-up only occurred if we added 3 % oxygen. Similar high m number instability effects during the dynamic phase had been observed in the pure theta pinch /9-13/, but the helical pinch seems to be more sensitive to turbulent preionization and/or high impurity concentration.

Since the plasma was generated and shock heated in a cylindrical quartz tube, we got a compressed plasma, which was initially also nearly cylindrical. With respect to the helical equilibrium position this corresponded to an $m = 1$ perturbation with a wavelength equal to the period length of the $\ell = 1$ field, exciting stable $m = 1$ oscillations about the equilibrium position.

With reduced preionization the stability of the helical plasma column was comparable to that of the theta pinch. Stereoscopic smear pictures for different parameters are given in Fig. 2.

The helical oscillations are readily seen. At late times the usual rotational theta pinch instabilities /11/ were observed. No significant deviation from the theta pinch could be found in the measured density profiles and plasma beta.

Comparing now with the equivalent case in exp. I, we can conclude that the gross behaviour is the same in both cases: The plasma helix is formed in the early phase, thus exciting stable oscillations around the helical equilibrium position. Differences are found only in details. For instance, the initial motion into the helical equilibrium during the dynamic phase seems to be more rapid in exp. I. This fact may be caused by the $\ell = 3$ harmonic field produced by the helical wires (see also cap. II).

3. Experiment III

The only difference between exp. II and exp. III lies in the fact that the small discharge tube is shifted into an eccentric position in exp. III (shift $\Delta = 3.7$ cm). By shock heating, a plasma column is generated concentric with the vessel, that is, eccentric with respect to the coil axis. Therefore, the total system is no longer helically symmetric. A similar situation may arise in toroidal geometry if the plasma is drifting or is generated away from the equilibrium position and also during the nonlinear development of a $m = 1$, $k \approx 0$ instability.

In exp. III a plasma helix is formed and strongly damped helical oscillations are seen, as in exp. II. The exact shape of the plasma column was determined from stereoscopic smear pictures at different slits along the coil (coil axis = z-axis). A projection of the centre line of the plasma column parallel to the coil axis is reconstructed point by point from these smear pictures. Some examples are shown in Fig. 3. The number at every point gives the distance between the midplane of the coil and the corresponding observation slit. Points with 60 cm relative distance have equal phase (helical wavelength $\lambda = 60$ cm) that is, the points $z = -30$, 30 and 210 cm, for instance, should

coincide. It is found that the total helix drifts away from the coil axis, but this drift is slower near the end (z = 210 cm), indicating some kind of stabilizing end effect.

Furthermore, the plasma helix seems to be rotated by about 10° relative to the helical magnetic axis of the vacuum field.

In Fig. 4 the radius of the plasma helix is plotted as a function of time. The oscillation frequency ω_{Hi} increases with increasing temperature and decreasing filling pressure. Damping occurs within several oscillation periods.

The formation of a helix in the eccentric position may be understood by observing the topology of the vacuum magnetic field: Each field line away from the helical magnetic axis is a helix itself, the centre line of which is tightly wound on a cylinder which is concentric with the coil. The pitch of this centre line corresponds to the rotational transform. But as mentioned in cap. II, the total rotational transform is very small ($\iota_{total} \approx 0.045$) and the latter effect is hardly detected experimentally.

If the plasma were to be generated concentrically and shifted out afterwards, we might get a slightly different situation because of the different history (e.g. different small forces from flux conservation of transverse fields).

Nevertheless, if we interpret the plasma acceleration as an unstable m = 1, k ≈ 0 movement resulting from the large initial disturbance (Δ = 3.7 cm), we can estimate a growth rate γ despite the relatively low temperature:
Assuming constant temperature and neglecting nonlinear effects, the unstable motion s(t) is given by

$$s(t) = s_0 \cdot \cosh(\gamma t) + \frac{v_0}{\gamma} \sinh(\gamma t) \quad ,$$

where in our case the initial values are $s_o = \Delta$ and $v_o = 0$.

Some results determined in this way are given in the following table:

Bank energy	0.5	0.5	0.5	1.5	MJ
Filling pressure	40	20	10	10	microns
$(T_i+T_e)_{max}$	50	100	200	600	eV
$\tau = 1/\gamma$	20	15	(15)	9.5	μs

The initial β value is 0.7 ... 0.9 and decreases during the discharge because of three-dimensional compression and end losses (see also sec. 4d, Internal probe measurements).

4. Experiment IV

In the last linear experiment a large diameter discharge tube was used which just fitted into the shaped coil. In this case the initial shock heating was much more effective and, therefore, an ion temperature in the keV region was achieved. Again no significant difference in plasma parameters was found between this experiment and previous theta pinch experiments using the same initial parameters.

In the high temperature regime, however, fast growing long-wavelength m = 1 instabilities were observed, whereas the short-wavelength helical mode again showed stably damped oscillation. The corresponding growth rate and the helical oscillation frequency were studied over a wide range of plasma parameters by varying the bank energy (0.5 ... 2.6 MJ) and the filling pressure (4 ... 40 μ).

Furthermore, we made discharges with reduced preionization energy and also with antiparallel bias field, resulting primarily in a decrease or increase of the mean plasma beta respectively.

In all discharges a thin plasma halo (density of a few $10^{14}[cm^{-3}]$, temperature of a few eV) outside the dense plasma column was observed which was generated by flute instabilities during the dynamic phase [14]. We emphasize that this plasma halo was more or less present in all our experiments on Isar I and we believe that it is unavoidable for theta pinches, at least for plasma parameters where stabilizing gyroradius effects are not very strong.

a) Experiments with standard preionization (see exp. II)

The degree of preionization was usually about $\alpha \approx 50$ % at the beginning of the main discharge. It was measured with a microwave interferometer (Michelson, $\lambda = 1$ mm).

The plasma radius at maximum magnetic field was about 10 mm and was nearly independent of the initial parameters (maximum compression ratio $\varkappa_{max} \approx 10$ with respect to the conducting wall). Correspondingly, the maximum density on the axis was nearly proportional to the filling pressure and was a few $10^{16}[cm^{-3}]$, the density profile being about Gaussian. The initial plasma beta on the axis was about 0.7 to 1, decreasing slowly for high temperature (two-dimensional compression) and faster for low temperature (three-dimensional compression; see sec. 4d, Internal magnetic probe measurements).

As in all preceding experiments, helical m = 1 oscillations (wavelength = length of the helical period) were triggered by the theta pinch compression in the cylindrical vessel. Their frequency ω_h was proportional to the temperature $\sqrt{(T_e+T_{i\perp})}$ over one order of magnitude, and the decay time was again of the same magnitude as the oscillation period (see also exp. III).

The radius of the plasma helix was between 1.0 and 1.4 cm (radius of vacuum magnetic axis r_m = 0.94 cm), the larger values corresponding to higher beta values.

Rapid m = 1 instabilities were observed for high temperature [$(T_{i\perp} + T_e) > 1$ keV; $T_{i\perp} > T_{i\parallel}$; $T_e \approx 400$ eV], the growth time being much less than the plasma lifetime. By means of stereoscopic smear pictures at different slits along the coil it was confirmed that the gross plasma motion had the same direction all along the coil, corresponding to a rigid sideward motion of the plasma helix. From statistics over many discharges the plasma motion was found to be preferentially away from the collector slit. This fact was possibly caused by small perturbations of the helical symmetry because of the finite length of the shaped coil, z-dependent plasma parameters, non-ideal quartz tube, and so on. As wall contact occurred nearly simultaneously (at equal phase) all over the coil, we conclude that there was no strong end effect in the high temperature regime.

With lower temperature [$(T_e + T_i) \lesssim 1$ keV, $T_e \lesssim T_i$], however, the plasma motion was more complicated and showed clear deviations from the exponential time dependence for large amplitude. In addition, the amplitude near the ends was sometimes smaller and the plasma did not hit the wall in contrast to the centre region, thus indicating a wavelength of twice the coil length.

With $(T_i + T_e) \lesssim 0.2$ keV no m = 1 instability was observed during the confinement time.
Typical smear pictures are given in Fig. 5 (right hand side). Numerical results are presented in Table 2, including the degree of preionization and the plasma beta on the axis averaged over the growth time of the instability. For this purpose the time dependence of beta was deduced from the plasma profile, from compensated magnetic loops, from the neutron rate and, for one case, from internal magnetic probe measurements (see 4. d). We give a range of the beta values rather than a fixed number because there is no definite averaging procedure and also because of the experimental error.

Table 2

Bank energy [MWs]	0.5		1.5			2.6	1.5		2.6	
Filling pressure [microns]	40	10	20	10	8	8	20	10	8	8
$(T_i + T_e)_{max}$ [keV]	(0.1)	0.5	0.5	1.3	1.6	2.1	0.5	1.3	1.9	1.6
ω_h [μs^{-1}]	1.2	2.4	2.6	4.2	4.4	5	2.6	4.2	~6	~6
$\gamma_{m=1}$ [μs^{-1}]	—	~0.08	0.1	0.3	0.5	0.6	—	—	0.3	—
$\gamma_{m=1}/\omega_h$	—	~0.03	0.04	0.07	0.11	0.12	—	—	~0.05	—
$\bar{\beta}_a$	0.5...0.7		0.5...0.8	0.6...0.9		0.7...0.9	0.5...0.7		0.5...0.7	0.4...0.6
α [%]	—	50	30	50	60	60	17	15	16	~11

If no value for γ and γ/ω_h is given then no instability was observed. Because of the connection of the plasma lifetime and Alfvén velocity this is generally the case when $\gamma/\omega < 0.03$, that is, a lower ratio cannot be measured with the present coil length and helical distortion.

b) Experiments with reduced preionization

By lowering the degree of preionization to about 15 % the instability was suppressed during the plasma lifetime for $(T_e + T_i) \leq 1$ keV, and for the highest temperature the growth time was doubled. From the plasma pressure and also from the excluded flux we conclude that the plasma beta had only decreased by about 20 %, while the plasma profile was only altered in details. With a further reduction of α no m = 1 instability could be seen at all. Results are also included in Table 2 and Fig. 5 (left hand side).

c) Experiments with antiparallel bias field and standard preionization

A very small antiparallel bias field was used to increase the plasma beta. With larger bias field a hollow density distribution was expected with $\beta = 1$ at the density maximum. As the compression ratio was ~ 10 (excluded flux ≤ 1 %) and the maximum field was 34 kG, a significant change in the density profile was expected for a bias field of the order of a few hundred gauss.

The results were as follows (10 microns, 1.5 MJ):

Bias field	0	-100 G	-360 G	-700 G
γ/ω_h	0.7	0.9	0.9	0.11

ω_h was nearly constant ($\omega_h \approx 4$ MHz).

The unstable mode was again a long-wavelength m = 1 mode. With even higher bias field a more complicated mode (possibly m = 0) with similar growth rate occurred. The maximum intensity of an oxygen V line also measured occurred earlier for higher bias field, thus indicating an increased electron temperature, and the neutron rate, which is very sensitive to the ion temperature in this regime, only decreased by a factor two.

Therefore, the main plasma parameters were only moderately changed, while the maximum beta approached unity, followed by the development of a hollow profile. These two effects must therefore have caused the slightly increased growth rate, but it is difficult to separate them.

d) Internal magnetic probe measurements

With a bank energy of 0.5 MJ, a filling pressure of 10 μ D_2, and standard preionization ($T_e \approx T_i \approx 250$ eV), we made internal magnetic probe measurements near the midplane of the coil. Figure 6 shows the geometrical arrangement. From these measurements we could derive magnetic field profiles and beta values for early times, where plasma cooling by the probe itself could be neglected. In Fig. 7 normalized profiles of the longitudinal B_z-field are shown for various times. The helical oscillations of the plasma are readily seen and agree well with the oscillations derived from stereoscopic smear pictures taken 150 cm away from that point. In Fig. 8 the value

$$\beta^* = \frac{B_{z,vac}^2 - B_{z,min}^2}{B_{z,vac}^2}$$

derived from the field profiles is given. $B_{z,vac}$ is the longitudinal magnetic field measured without plasma in the discharge tube, while $B_{z,min}$ is the longitudinal field on the plasma axis. For $t \geq 3\mu s$ the compression oscillations are

damped out and to lowest order

$$\beta^* \approx \beta_{max} \approx 2\mu_0 \cdot p_{max} / B^2_{z,vac}$$

(p = plasma pressure perpendicular to the field lines). There is no chance of deriving the rotational transform inside the plasma from the field components measured only along one line. There is, however, an interesting feature in the B_y-profile. In Fig. 9 the B_z-profile and the profile for

$$\Delta B_y = B_{y,plasma} - B_{y,vac}$$

are given for the second expansion of the plasma column ($t \approx 2$ µs), again normalized to the longitudinal field without plasma. One finds that during the first few microseconds ΔB_y has a complicated structure in the outer region. This indicates that longitudinal or helical currents were also flowing outside the dense column. Later on these currents were more and more concentrated near the centre column. But again one could not derive the exact current distribution.

A more detailed investigation of the dynamic phase showed that flute-like instabilities developed because of the high dynamic forces connected with the shock heating and the subsequent compression oscillations. These instabilities reached amplitudes of the order of the plasma radius itself and sometimes plasma even split off to form the thin plasma halo described elsewhere /14/.

At the beginning of the adiabatic phase these flute modes disappeared, that is, they were not unstable modes of the static equilibrium.

Returning now to the field measurements, it seems quite likely that the measured currents are helical mirror currents on flute modes or possibly on split-off filaments. It should be noted that helical mirror currents are not force-free and cannot flow in the nearly pressureless halo.

On the other hand, if we interpret these currents as force-free longitudinal currents, then a return current on the centre column, for instance, is necessary for the net longitudinal current to be zero (see also the following section).

5. Longitudinal currents and rotational transform

If there is no connection between the end plates of the linear discharge vessel, then the net longitudinal current is, of course, zero. In a toroidal device, however, a plasma current can be induced by the helical fields because of their rotational transform and, therefore, we shall look at this problem in more detail. As we use a crowbarred z-discharge for preionization in the linear experiment (see Fig. 1), the end plates are, indeed, connected by an external circuit. In general, however, small remaining z-currents are suppressed by a voltage-dependent resistor in series (thyrites) and, therefore, this connection has high resistance for low voltages (a few kilovolts).

In order to investigate the effect of the helical field, we carried out two modifications:

a) Induced voltage

First we measured the induced voltage across the nonlinear resistance while the current was about zero. It turned out that the induced voltage as a function of time was nearly proportional to the coil voltage (Fig. 10a).

b) Induced current

Then we removed the thyrites and the longitudinal current (Fig. 10b) flowing was now measured. As expected, this current was about proportional to the main theta current and, therefore, also to the helical field (shaped coil!). The unstable plasma motion was not seriously altered by this comparatively small current.

In order to understand these results, we make the following model:
It is assumed that an infinitely conducting plasma column is established during preionization and the end plates are shorted (no thyrites). When the main field is now triggered, an azimuthal flux χ is set up proportional to the rotational transform ι and the longitudinal flux ϕ. From conservation of flux in the closed circuit (plasma and external conductor, total inductance L) we find a net current I_z

$$\frac{dI_z}{dt} \approx \frac{1}{L}\,\frac{d\chi}{dt} = \frac{1}{L}\,\frac{d\phi}{dt}\cdot\langle\iota_{coil}\rangle$$

With thyrites we get an induced voltage U_z

$$U_z \approx \frac{d\chi}{dt} = \frac{d\phi}{dt}\cdot\langle\iota_{coil}\rangle = U_{coil}\cdot\langle\iota_{coil}\rangle$$

$\langle\iota_{coil}\rangle$ is the total rotational transform averaged over the cross section. The total rotational transform of the vacuum magnetic field is $\iota \approx 0.045$ near the axis, slowly increasing with radius to $\iota \approx 0.1$ at the wall. Additional contributions come from the helical mirror currents in the finite β plasma column, thus resulting in a very high rotational transform near the plasma surface. Taking only the vacuum rotational transform, we find

$$U_{z\,max} \approx 2\ kV\ ,\quad I_{z\,max} \approx 1\ kA\ .$$

Comparing with the experimental curves we find agreement in phase, while the experimental values are about a factor of two higher than expected qualitatively for a high beta plasma.

In a toroidal system this current must be compensated by an externally induced current /3/.

But while it is possible to compensate the net longitudinal current, it is very difficult to control the net current on each magnetic surface, which, in general, is set equal to zero in relevant theoretical models.

E. Discussion of plasma equilibrium and stability

In the following discussion we are mainly concerned with helical equilibrium and with stability effects which are closely connected with the helical field. That is, we exclude other theta pinch instabilities such as mirror instabilities /10/ observed again for high temperature and anisotropic velocity distribution.

We compare the experimental results with improved sharp boundary theories and also with theories using diffuse pressure profiles. Because of the finite length of the linear system we also include end effects.

We use the following Fourier expansion to describe the deviation of the plasma surface (or of any other flux surface) from a circular cylinder:

$$r(\theta, z) = r_0 \left[1 + \sum_{\ell=0}^{\infty} \delta_\ell \cos \ell(\theta - hz)\right], \quad \delta_\ell \ll 1 \quad *)$$

1. Helical equilibrium

In all experiments the plasma was found to form a helix near the helical magnetic axis of the $\ell = 1$ vacuum magnetic field. The sharp boundary model predicts a helix radius r_h weakly dependent on beta /15/

$$r_h = r_p \cdot \delta_1 = \frac{\tilde{B}_{r1}}{B_z \cdot h \cdot (1 - \frac{\beta}{2})} = \frac{r_m}{(1 - \frac{\beta}{2})}$$

$\tilde{B}_{r1}$ is the maximum of the radial magnetic field near the axis and r_m the radius of the magnetic axis of the vacuum field which is $r_m = 0.94$ cm for the shaped coil. Since the experimental density profile is Gaussian, we expect that the sharp boundary theory predicts too high a plasma deflection, if the beta on the axis is used. Indeed, for $\beta_{exp} \approx 0.4 \ldots 0.9$ we find $r_{h,exp} \approx 1.0 \ldots 1.4$ cm, while the sharp boundary model gives $r_h \approx 1.2 \ldots 1.7$ cm.

---

*) With large helical shift (helix radius $r_h \geq r_o$) the Fourier expansion has to be done in a helical coordinate system (for $\ell \neq 1$) and δ_1 is defined by $\delta_1 = r_h/r_o$ (see [16, 18]).

Furthermore, no $\ell = 1$ equilibrium with circular cross section (no z-current) is found in the sharp boundary theory, if /16/

$$\beta \cdot \delta_1 > \pi^2/16 \approx 0.6$$

But while $\beta \cdot \delta_1 \gtrsim 0.6$ for most experimental parameters, a well confined helical plasma column is observed in all cases, and the plasma cross section is circular within the experimental error.

We may also draw a comparison with the more realistic helical equilibrium given by Nührenberg /17+)/, where a smooth pressure profile is used and an elliptical deformation is allowed in second order. The numerical example in /17/ (circular boundary cross section, $hr_{coil} \sim 1$, $\varkappa \approx 6$, $\beta_{max} \approx 0.6$) fits with the gross experimental parameters except for the smallness parameter ϵ ($\epsilon_{example} = hr_h = 0.2$, $\epsilon_{exp} \approx 0.1 \ldots 0.14$). Since the helical distortion scales with ϵ^2, we calculate for our case a maximum $\delta_{2max} \approx 0.2 \ldots 0.1$ at that radius, where the pressure gradient is maximum. But for nearly Gaussian experimental pressure profiles the maximum gradient is much smaller, possibly resulting in smaller δ_2.

Experimentally, however, it is difficult to detect a $\delta_2 < 0.1$ and, therefore, there is no real contradiction between experiment and existing theories.

2. Helical oscillations ($m=1$, $k=h$)

Since the plasma is generated and compressed in a cylindrical vessel, we produce an initial m = 1 disturbance from the helical equilibrium and as a consequence helical oscillations with wavelength equal to the helical period were observed.

+) The scaling in /17/ is more general in one sense than in existing sharp boundary theories. While in /17/ only the product $hr_h = hr_p \cdot \delta_1$ is small and there is no restriction on δ_1/hr_p, in sharp boundary models $\delta_1 \ll hr_p \approx 1$ (old theory /4/) or $hr_p \ll \delta_1 \approx 1$ (new ordering /18/) is assumed.

Looking at the δW, which is given explicitly in the next section, it turns out that for this mode all terms arising from the helical field are negligible and the remaining term is the usual kink mode term of the theta pinch. Because of the high compression ratio ($\varkappa \leq 10$) this mode is not affected by the wall. Thus, we get the helical frequency (sharp boundary)

$$\omega_h^2 = (2-\beta)\, h^2 V_A^2 \quad ,$$

where v_A is an Alfvén velocity calculated with the density on the axis and the magnetic field outside. Using $\beta = 2\mu_o n k (T_e+T_i)/B_a^2$, we write ω_h as a function of the ion and electron temperatures

$$\omega_h^2 = \left(\frac{2-\beta}{\beta}\right) \cdot h \cdot \frac{2k(T_e+T_i)}{m_i}$$

(k = Boltzmann's constant, m_i = ion mass).

Comparing now this sharp boundary result with the experiment (Fig. 11), it turns out that all experimental values lie between $\beta \approx 0.4$ and $\beta \approx 1$, where the frequencies measured with the small discharge tube (shaped boxes) correspond to lower beta. Differences to the experimental beta on the axis may again be explained by the smooth pressure profile.

In all cases it is found that the helical oscillations are damped within several oscillation periods (see Fig. 4). We suppose that the kinetic energy of the oscillation is transferred to modes with high wave number and/or frequency by phase mixing /19/ because of the diffuse profile and is finally converted to internal energy.

Using a small superposed helical current in resonance with the oscillations, one might get efficient plasma heating at moderate and technically feasible frequencies. As the initial kinetic energy of the helical oscillation is several per cent of the thermal energy, we get a reasonably high heating rate. A detailed treatment of this problem, including the damping of the $m = 0$, $k \approx 0$ compression oscillations, will be given elsewhere /20/.

3. m = 1, long-wavelength instability

Until now stability calculations for the long-wavelength m = 1 mode including explicit growth rates have only been done with the sharp boundary model. It is generally believed that this model gives a fairly accurate description for this mode.

We take the advanced theory of Freidberg /16/, which in the appropriate limits represents the results obtained in the old /4,15/ and new /18/ ordering. It turns out that Freidberg's numerical results are quite close to the old ordering except for $\beta \approx 1$. Thus, we can utilize the δW of the old ordering as an analytical approximation, though the new ordering is valid for our experiment.
For $k \longrightarrow 0$ we get for the growth rate

$$\gamma^2_{k\to 0} = h^2 v_A^2 \left[h^2 r_p^2 \delta_1^2 \frac{\beta(4-3\beta)}{8(1-\beta)}(2-\beta) - \delta_1^2 \beta^2 \frac{1}{\varkappa^4} \right], \quad \varkappa = \frac{r_{wall}}{r_p}$$

Since $\varkappa \approx 10$, the second term is negligible.
For finite wavelength the stabilizing kink mode term must be added, which for distant wall reads

$$\gamma^2_{kink\,mode} = -(2-\beta) k^2 v_A^2, \qquad k r_p \ll 1, \; k r_{coil} \gtrsim 1$$

(k = wave number of the instability).
This limit is valid except for very low compression ratio, where an additional small wall effect appears /21/.
Keeping only the major terms, we then get

$$\gamma^2 = (h v_A)^2 \cdot (h r_p)^2 \cdot \delta_1^2 \left[\frac{\beta(4-3\beta)(2-\beta)}{8(1-\beta)} \right] - k^2 v_A^2 (2-\beta)$$

We examine two cases:
Firstly, we take $k \longrightarrow 0$, that is, we neglect end effects and the only remaining term is the destabilizing stellarator term.

But we have seen experimentally that, at least for low temperatures and small growth rate, end effects are present though it is difficult to find a quantitative measure. Therefore, we try the case where the plasma column is fixed at the ends of the coil, that is, we take the wavelength to be about twice the coil length.
Since the unstable term is about proportional to beta, while the kink mode term varies with $(2-\beta)$, we now get a critical beta <u>below</u> which the plasma is stable (here $\beta_{crit} \approx 0.4$). This is in contrast to the dipole wall effect, present also for $k \longrightarrow 0$, which, for low compression ratio, gives a critical beta <u>above</u> which stability is obtained.

Experimentally, we measure γ and ω_h, which are both proportional to V_A and, for constant beta, proportional to $\sqrt{T_e+T_i}$. Taking the ratio γ/ω_h, therefore, we get a normalized growth rate which has to be compared with the theoretically expected ratio

$$\frac{\gamma^2}{\omega_h^2} = h^2 r_h^2 \frac{\beta(4-3\beta)}{8(1-\beta)} - \frac{k^2}{h^2} \quad , \quad r_h = r_p \cdot \delta_1$$

In Fig. 12 we compare the experimental growth rates with Freidberg's numerical results (full lines), for which the above expression (dashed lines) is a reasonable analytical approximation for $\beta < 0.9$, as mentioned earlier.
We see that for $\gamma/\omega_h \gtrsim 0.1$ end effects are of minor importance and the experimental data are close to the theoretical curves. But for $\gamma/\omega_h \ll 0.1$ the experimental growth rates are even slightly lower than theoretically expected with fixed ends.

Furthermore, by fixing the ends we overestimate the end effects and, therefore, we conclude that the experimental growth rates, at least for intermediate beta, are clearly lower than expected from sharp boundary theory including realistic end effects.

Such a difference may be explained by means of simplifying assumptions in the theoretical model (e.g. circular cross section). The most significant difference is that, experimentally, the pressure profile is smooth, and taking the beta on the axis, although it is appropriately time averaged for comparison, may result in too high growth rates.

We emphasize that this stabilizing kink mode term may be important for toroidal systems with superposed helical fields (ℓ = 0,1,2,3) and with a total rotational transform of the order one: If the rotational transform is adjusted in such a way that the most unstable mode is not an eigenmode of the system (periodicity condition), then a kink-mode-like term is expected, thus resulting in a finite critical beta, as shown in the linear case with end effects. For the ℓ = 1 system the rotational transform and the corresponding term in δW are formally too small and do not appear in the above formulas.

Finally, we note that it has recently been shown /22/ that helically symmetric equilibria with diffuse pressure profile exist which satisfy a sufficient stability criterion below a finite critical beta (no small beta expansion). Since a free plasma boundary is assumed this criterion also includes m = 1 stability. These equilibria are characterized by additional elliptical and triangular deformations of the plasma cross section and are not found by a small parameter expansion, where the zeroth order is the theta pinch.

This class of equilibria and the analogous toroidal equilibria are equally interesting and should be further investigated.

4. m ≥ 2 modes

Sharp boundary theory predicts first order instability for all modes with m ≥ 2 and long axial wavelength /23/. It is expected, however, that finite gyroradius corrections are important for typical parameters and that ideal MHD theory gives pessimistic results for these modes.

By using a Vlasov fluid model, Freidberg /24/ has indeed shown that, while the stability threshhold is the same as in ideal MHD, the growth rate becomes exponentially small for the $m \geq 2$ modes if typical theta pinch data are assumed.

At first glance this is in agreement with the experimental fact that no $m \geq 2$ instabilities are observed during the adiabatic phase.

But, in addition, we have found that $m \geq 2$ perturbations of the plasma column, produced during the dynamic phase, are even damped away within several microseconds, that is, these modes are stable and do not slowly become unstable.

Furthermore, by varying the filling pressure and bank energy we obtained plasma parameters where the ions were collision-free as well as collision dominated with respect to the ion gyro-period ($0.25 < \tau_{ii} \cdot \omega_{ci} < 10^3$, τ_{ii} = ion ion collision time, ω_{ci} = gyro-frequency). For the collision dominated case gyro radius effects will be substantially reduced, but again no growing $m \geq 2$ instabilities are observed.

Obviously, additional stabilizing effects, not included in the Vlasov fluid model, must be present in such a way that the threshhold is substantially shifted and the high m number modes become stable.

There are several possibilities for damping and/or stabilizing processes in a real diffuse theta pinch plasma including also all kinds of end effects (e.g. shorting of the electric Hall field /11/). Additional stabilization is expected because of the high shear produced by the helical field in connection with the smooth density profile.

Finally, we should again note that within the scope of ideal MHD finite beta helical equilibria have been found /22, 27/, which satisfy necessary (local) or even sufficient stability criteria.

F. Conclusions and prospects

We have shown experimentally that a dense plasma column with helical $\ell = 1$ symmetry can be established and effectively heated by fast compression.
We have studied the equilibrium and stability of this helical pinch for a wide range of plasma parameters.

The equilibrium parameters have been found to be in good agreement with existing high beta theories.

Helical $m = 1$ oscillations were observed in connection with the formation of the helical equilibrium. Their frequency is that of the usual theta pinch kink mode (wavelength = helical period). These oscillations are damped away within several oscillation periods by phase mixing as a consequence of the diffuse pressure profile.

This damping mechanism should also provide effective plasma heating for finite beta plasmas at moderate and technically feasible frequencies.

For present parameters the helical equilibrium is unstable to long-wavelength $m = 1$ perturbations. The growth rates are somewhat lower than predicted by the sharp boundary theory including realistic end effects.

The $m \geq 2$ instabilities also predicted by the sharp boundary theory were not observed. On the contrary, $m \geq 2$ perturbation produced during the dynamic phase disappeared in the adiabatic phase.
A simple Vlasov fluid model which gives reduced growth rates but retains threshhold is not sufficient to explain this fact.

The main purpose of the linear experiments described above was to gain experience for a toroidal confinement experiment where an appropriate combination of helical fields will be used to overcome the toroidal drift force. Since the toroidal current will be zero, such a system might easily be operated in the steady state.

We have proved that shock heating is a very convenient method for generating fusion-like high-beta plasmas in more complicated geometries as well, and we shall also use it in future experiments. Nevertheless, we have also shown that there are other mechanisms in a diffuse high-beta plasma, promising efficient plasma heating at moderate and technically feasible frequencies.

A big toroidal experiment on ISAR 1 (called Isar T 1) with a $\ell = 1$ field in leading order and small $\ell = 2$ and $\ell = 0$ fields (to provide the toroidal equilibrium) is now under way.

Acknowledgment

The authors gratefully acknowledge discussions with F. Herrnegger, W. Grossmann and J. Nührenberg. They also wish to thank M. Münich for the microwave measurements and R. Wunderlich for his assistance with the data processing.

References

1 M. Kaufmann, E. Fünfer, J. Junker, J. Neuhauser; Report IPP 1/111, Institut für Plasmaphysik, Garching, (1970)

2 M. Kaufmann, E. Fünfer, W. Lotz, J. Neuhauser; Contribution to the Fourth European Conference on Controlled Fusion and Plasma Physics, Rome (1970), p. 39

3 E. Fünfer, M. Kaufmann, W. Lotz, J. Neuhauser; Plasma Physics and Controlled Nuclear Fusion Research, IAEA Vienna (1971), Vol. III, CN28/J-3

4 H. Grad, H. Weitzner; Phys. Fluids 12, 1725 (1969)

5 F. L. Ribe; Los Alamos Scientific Laboratory Report LA-4098 (1969)

6 S. C. Burnett et al.; Plasma Physics and Controlled Nuclear Fusion Research, IAEA Vienna (1971), Vol. III, CN28/J-4

7 G. Lehner, F. Pohl; Report IPP 1/119, Institut für Plasmaphysik, Garching, (1971)

8 R. Wilhelm; Z. Physik 222, 208 (1969)

9 Report in preparation

10 M. Kaufmann, J. Neuhauser, H. Röhr; Z. Physik 244, 99 (1971)

11 M. Kaufmann, E. Fünfer, J. Junker, J. Neuhauser, U. Seidel; Report IPP 1/123, Institut für Plasmaphysik, Garching (1971)

12 J. Neuhauser; Z. Physik 245, 361 (1971)

13 W. Braun, M. Kaufmann, H. Röhr, W. Schneider; Verhandl. DPG (VI) 5, 68 (1970)

14 J. Freund; Z. Physik 258, 108 (1973)

15 F. L. Ribe, M. N. Rosenbluth; Phys. Fluids 13, 2572 (1970)

16 J. P. Freidberg; Phys. Fluids 14, 2454 (1971)

17 J. Nührenberg; Phys. Fluids 13, 2082 (1970)

18 H. Weitzner; Phys. Fluids 14, 658 (1971)

19 W. Grossmann, J. Tataronis; Proc. 2nd Topical Conference on Pulsed High-Beta Plasmas, W. Lotz, Ed., Garching (1972), IPP 1/127, B 6

20 W. Grossmann, M. Kaufmann, J. Neuhauser; to be publ. in Nucl. Fusion

21 R. Lüst et al.; Phys. Fluids 4, 891 (1961)

22 D. Correa, D. Lortz; Proc. 2nd Topical Conference on Pulsed High-Beta Plasmas, W. Lotz, Ed., Garching (1972), IPP 1/127, B 3

23 M. N. Rosenbluth et al.; Phys. Fluids 12, 726 (1969)

24 J. P. Freidberg; Phys. Fluids 15, 1102 (1972)

25 E. Fünfer, M. Kaufmann, W. Lotz, M. Münich, J. Neuhauser, G. Schramm, U. Seidel; Proc. 2nd Topical Conference on Pulsed High-Beta Plasmas, W. Lotz, Ed., Garching (1972), IPP 1/127, A 2

26 F. Meyer, H. U. Schmidt; Z. Naturforsch. 13a, 1005 (1953)

27 V. D. Shafranov, E. I. Yurchenko; Nucl. Fusion 9, 285 (1969)

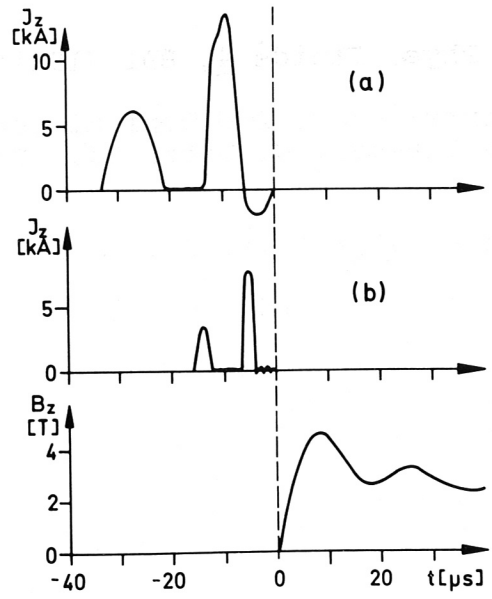

Fig. 1 Z-pinch preionization:
Z-current pulses for original (a) and reduced (b) preionization energy.

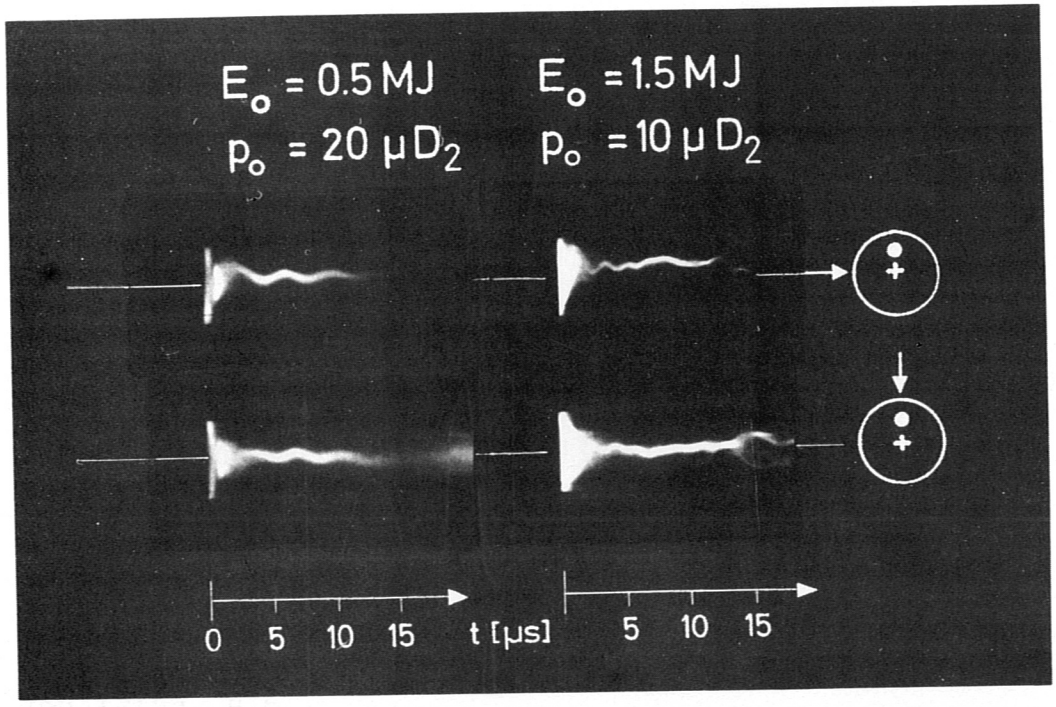

Fig. 2 Exp. II: Stereoscopic smear pictures for different parameters.

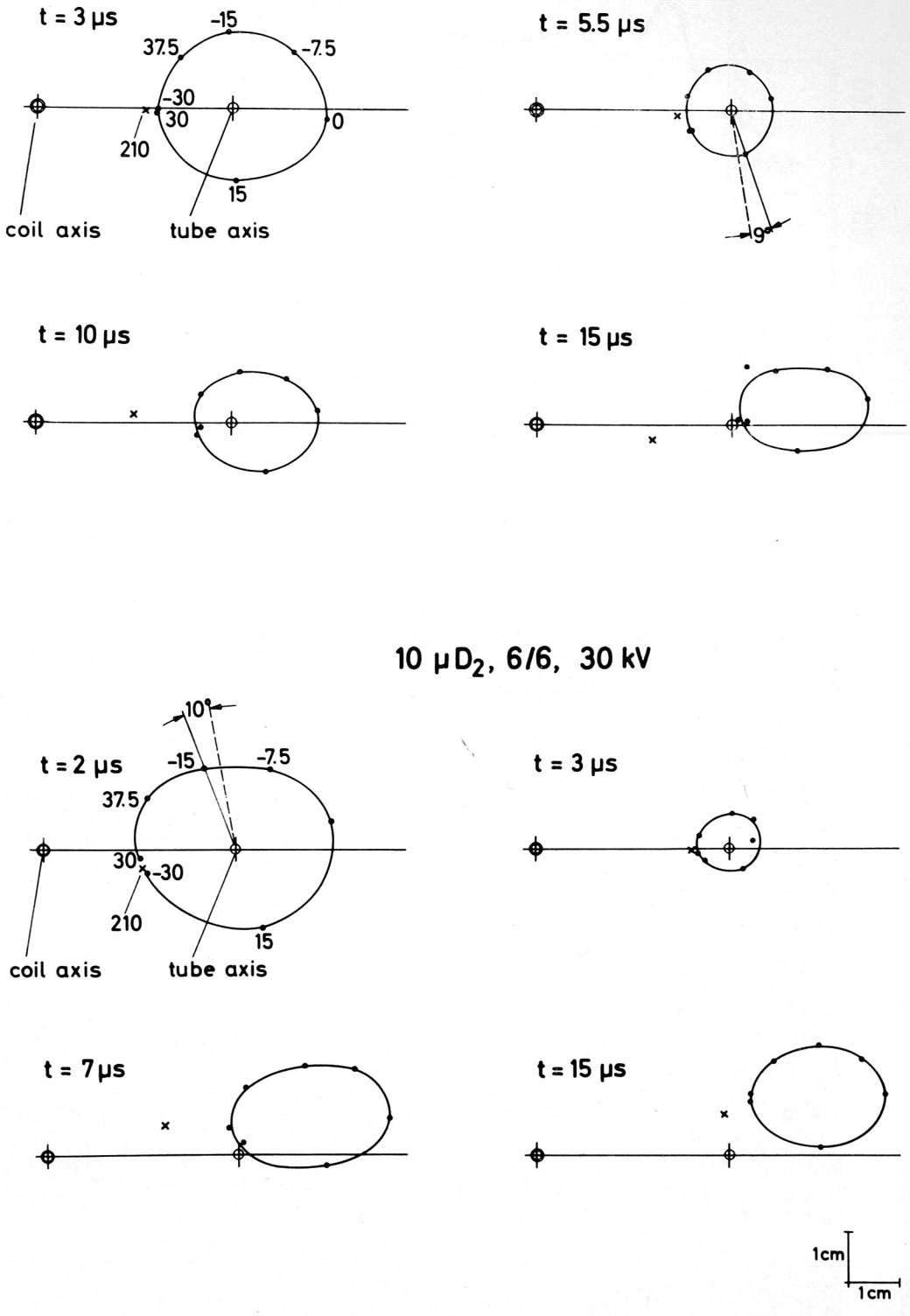

Fig. 3 Exp. III: The centre line of the plasma helix as seen from the coil end (the numbers indicate the distance [cm] from the midplane).

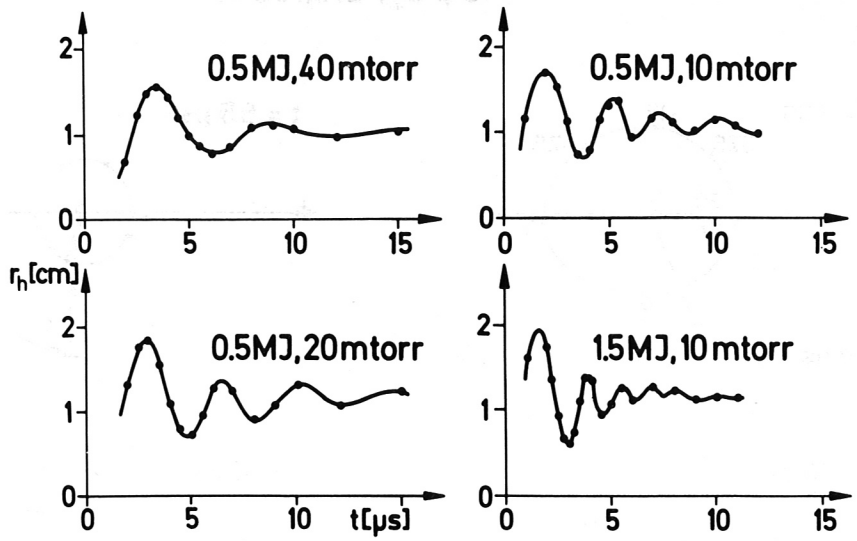

Fig. 4 Exp. III: The radius of the plasma helix is shown as a function of time.

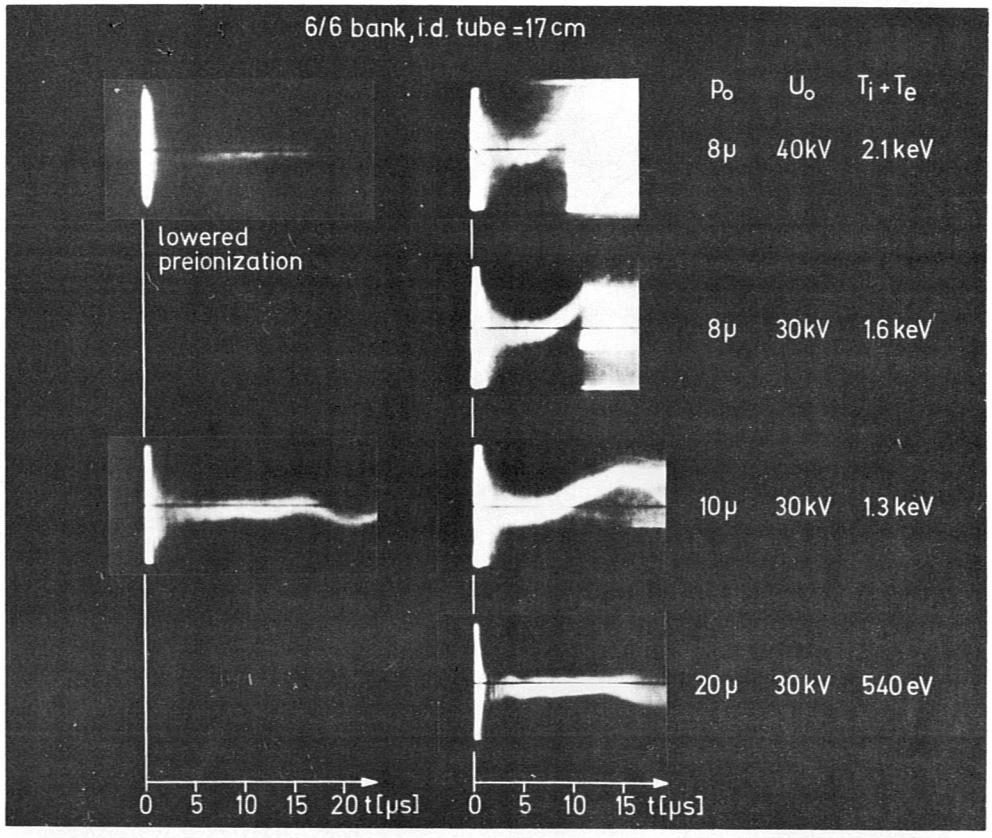

Fig. 5 Exp. IV: Smear pictures showing m = 1 instabilities for various parameters (right hand side: $\alpha \approx 50$ %, left hand side: $\alpha \approx 15$ %).

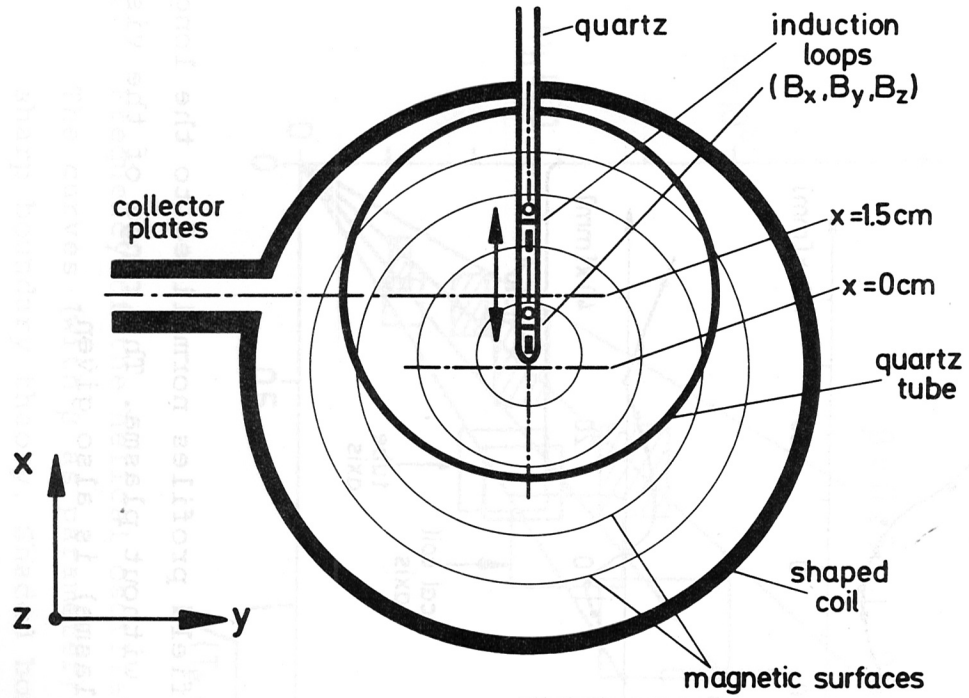

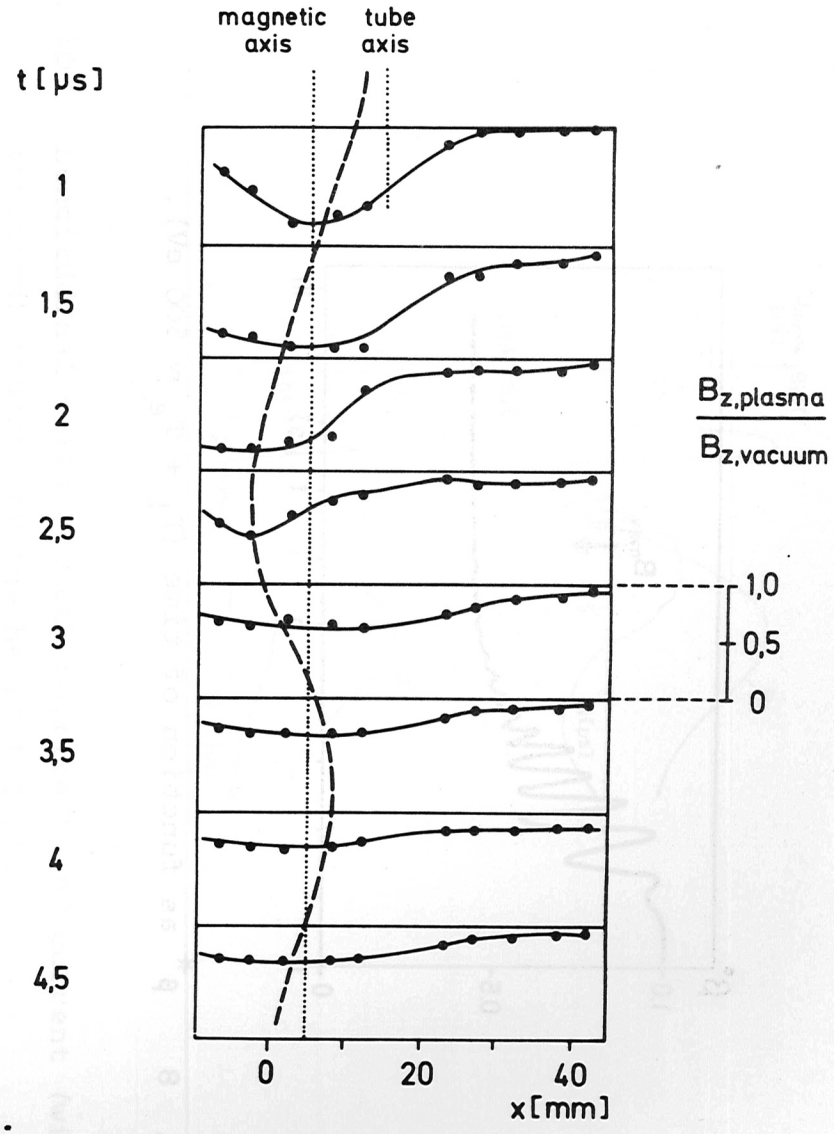

Fig. 6 Internal magnetic probe measurements (schematic).

Fig. 7 Normalized profiles of the longitudinal field. The dashed line shows the helical oscillations. →

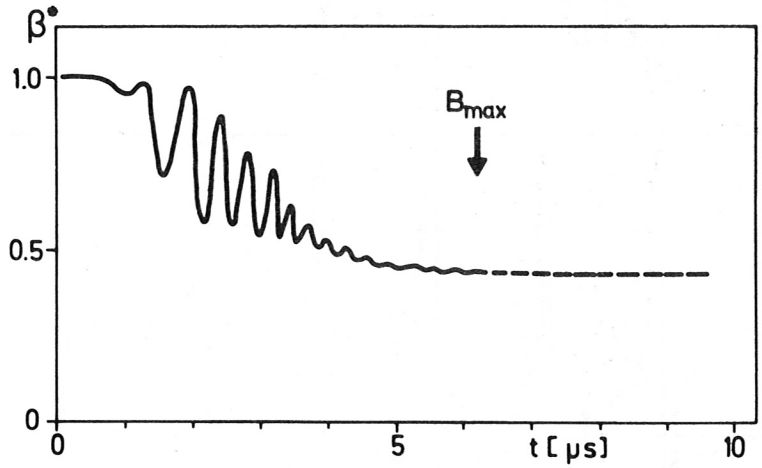

Fig. 8 β^* as function of time ($T_i + T_e \approx 500$ eV).

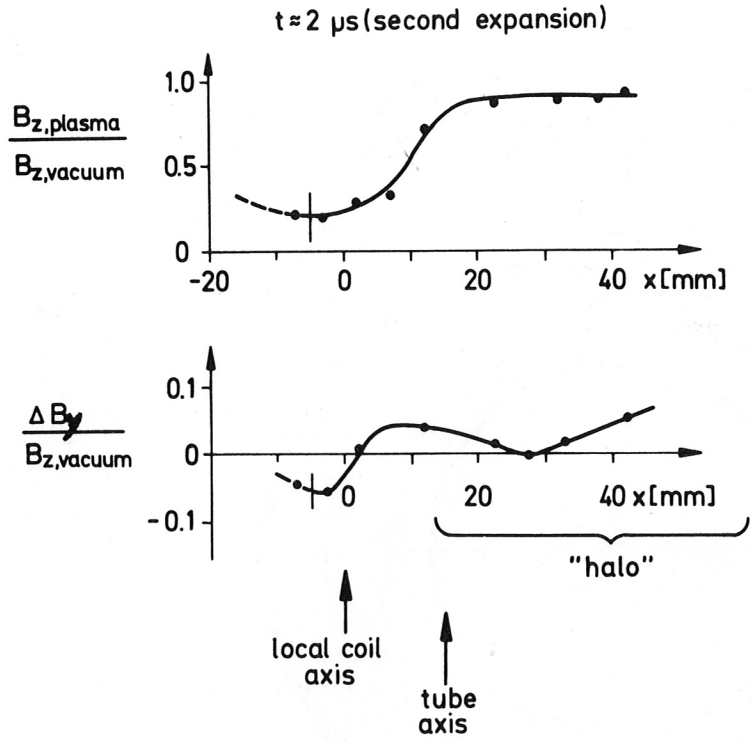

Fig. 9 Comparison of field profiles normalized to the longitudinal field measured without plasma. The range of the visible "halo" (thin plasma) is also given.

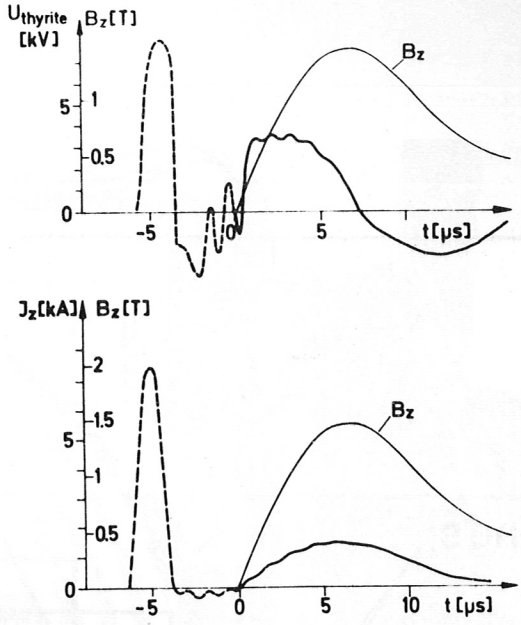

Fig. 10 Longitudinal voltage (with thyrites) and current (without thyrites) induced by the helical field.

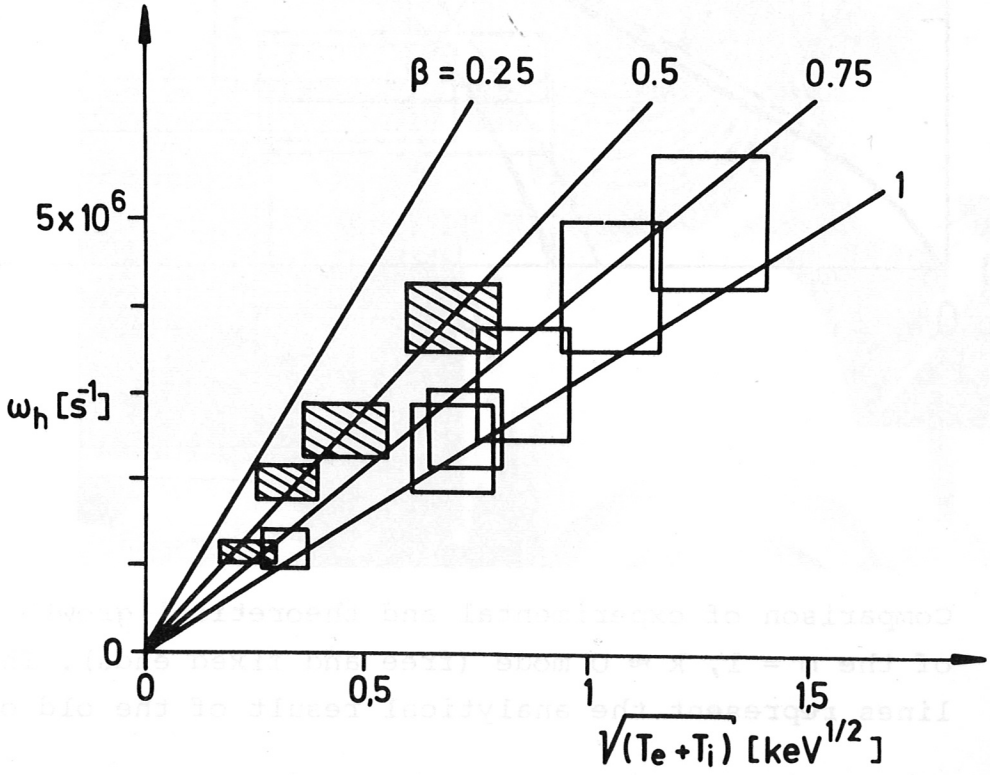

Fig. 11 Frequency of the helical oscillations versus $\sqrt{T_e + T_i}$. The curves (with β as parameter) are calculated from sharp boundary theory. Shaded boxes correspond to the small discharge tube (Exp. II and III).

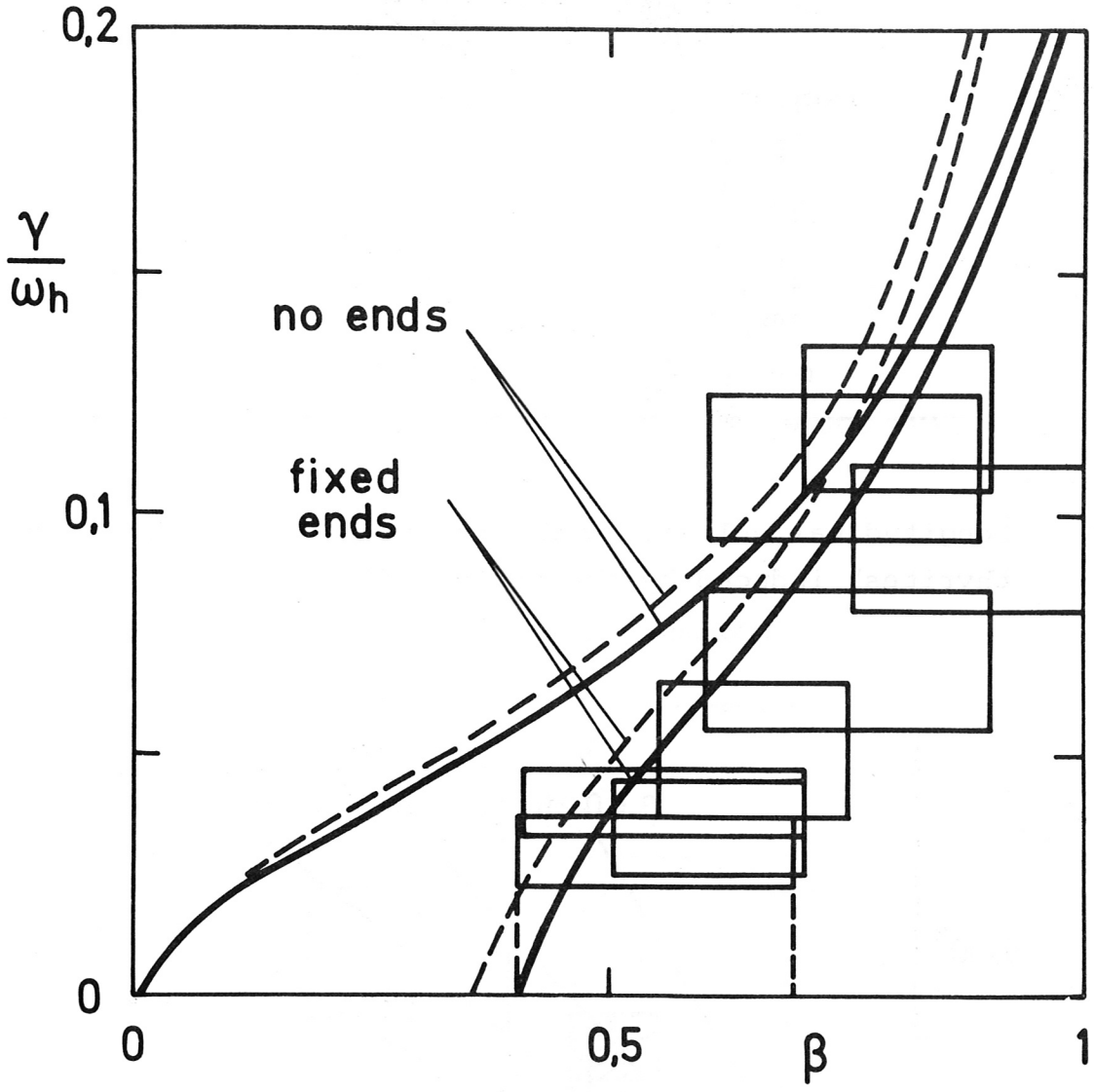

Fig. 12 Comparison of experimental and theoretical growth rates of the m = 1, k ≈ 0 mode (free and fixed ends). The dashed lines represent the analytical result of the old ordering.

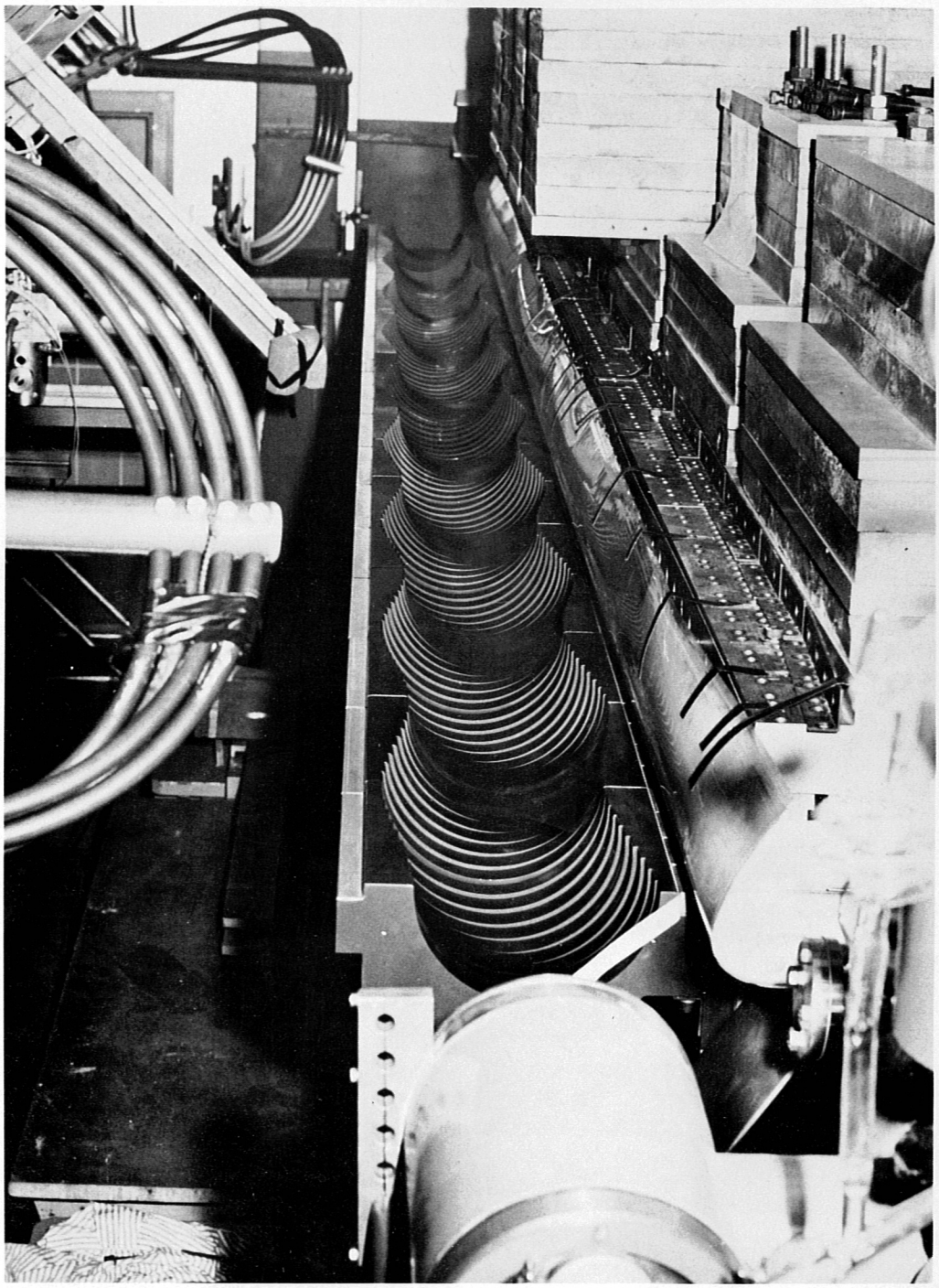

Fig. 13 Helically shaped theta coil (upper part removed)